5th International Conference on COMPUTATIONAL STRUCTURES TECHNOLOGY
Leuven, Belgium, 6-8 September 2000

# Swaged bolts: Modelling of the installation process and numerical analysis of the mechanical behaviour

M. Dréan[1], A.-M. Habraken[2], A. Bouchaïr[1] and J.-P. Muzeau[1]

## Abstract

Swaged bolts are an alternative to high strength (HS) bolts for connections in steel structures. To clarify the different steps involved during their specific installation process, a numerical modelling has been carried out. It allows the relevant phenomena to be described and to be evaluated. This numerical calculation accounts for mechanical plasticity and friction contact between the components of swaged bolts. The finite element code "Lagamine" designed for the forming analysis that requires the modelling of the friction between plastically deformable solids has been used with an original and quite efficient way to take into account the contact. The drawing of the stress distributions during and after the swaging process is the main result of this research.

## 1 Introduction

Swaged bolts are an alternative to high strength (HS) bolts for connections in steel structures. Because of their automatic installation process, the installed preload is expected to be established with a reasonable confidence. If a better knowledge about this fastener raised from the tests which have been carried out to qualify the bolts in Europe [1, 2, 3], the difficulty to understand, in detail, the different steps of the installation process appeared. Therefore, it was decided to use a numerical modelling to describe and to evaluate the phenomena.

In a first step, the bolt itself is presented. Then, the software «Lagamine» is described which allows practical applications with large strains, large rotations and/or large displacements to be calculated, accounting for friction between elements. After the careful detailing of the modelling of each bolt component (geometry and mechanical characteristics), the results of the calculation are given. They include both the load transfer and the stress distributions, which are evaluated at each step of the installation process. Stress concentrations, for instance, are determined which explain the behaviour of swaged bolts under fatigue.

## 2 General presentation of swaged bolts

### 2.1 Description of the basic components

As classical HSFG bolts, prestressed swaged bolts are constituted by two different components (Figure 1): a pin, with a hexagonal head, which acts as the screw, and a collar, which acts as the nut. The available pin diameters are 12, 16, 20, 24 and 27 mm. Their geometrical properties and mechanical characteristics are comparable to those of high-strength bolts grade 10.9 or A490. If more detailed information is required, see Czarnomska *et al* [1]. One of the geometrical characteristics of these bolts are the helical grooves which look like a thread but with a special shape. It is made up of a succession of linear and elliptical parts different from a classical thread. The groove shape has angles of 20° and 40° and not of 30° as it is in a traditional thread.

### 2.2 Installation process

The installation process of swaged bolts represents their main difference compared to classical bolts but also their major advantage. It consists in swaging the collar onto the pin with a special hydraulic tool. The internal diameter of the nose assembly, the anvil, is smaller than the external diameter of the collar. That forces the collar material to flow into the pin grooves.

The sequence of the installation process can be divided into four steps (Figure 2). First, the pin is inserted through a prepared hole and the collar is twisted on the pin with a unique small thread called tab-lock (**1**). The hydraulic tool is placed over the pintail and the anvil comes in contact with the collar. Then, the hydraulic pressure leads the tool to pull on the pintail and the anvil to push the collar, in order to draw the work pieces together (**2**). Continued pulling on the pintail moves the anvil forward, swaging the collar into the lock grooves. Controlled swaging lengthens the collar that develops a permanent clamp force in the pin. When swaging is completed (**3**), the pintail separates from the pin and the anvil disengages from the collar (**4**).

This automatic and rather fast installation process allows a clamp force, the preload, to be installed when the connected plates respect the out-of-flatness tolerances. Nevertheless, some tests have been carried out to check the quality of the installed preload, Missoum [2], Baptista *et al* [3] and it appears that, in case of lack of flatness, a large gap between the connected plates affects the value of the installed preload. Therefore, it has been decided to investigate the mechanical behaviour of the pin and the collar during the swaging phases. With this aim, a FEM modelling has been used in association with an adequate mesh of each component of a bolt.

[1] LERMES - CUST, Blaise Pascal University, Clermont-Ferrand, France
[2] MSM, University of Liège, Liège, Belgium

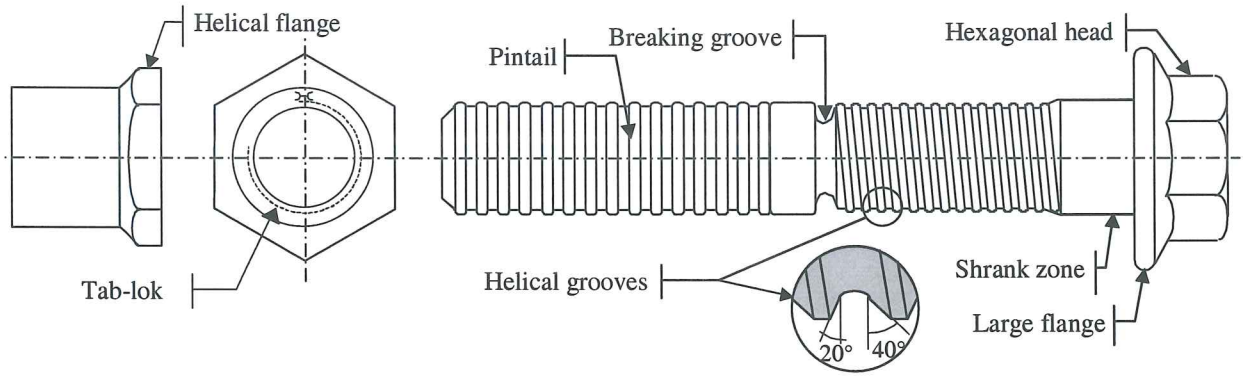


Figure 1: Collar and pin of a swaged bolt

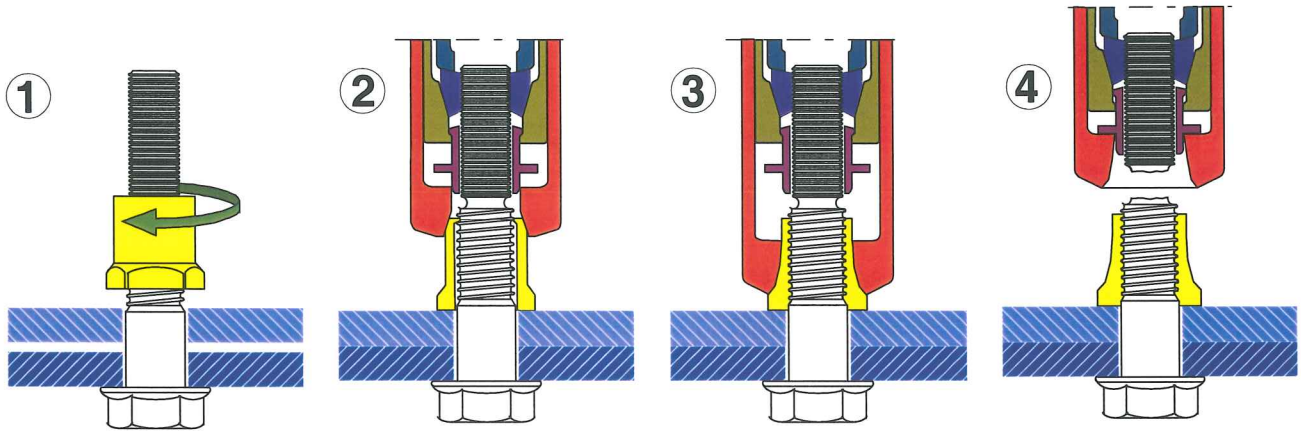


Figure 2: Installation process

# 3 General presentation of the finite element code «Lagamine»

## 3.1 Introduction

The software «Lagamine» has been developed at the University of Liege by Cescotto's team allowing practical applications with large strains, large rotations and/or large displacements to be studied. It allows problems related to hot and cold rolling, deep drawing, extrusion or forging processes to be analysed. It includes both solid and contact finite elements as well as a large library of constitutive laws: isotropic or anisotropic elastoplastic laws of associated type or not, with or without dilatance, elastoviscoplastic or damage laws. The modular architecture of the code allows any new element or new laws to be easily added. The set of non-linear equations is solved by incremental iterative process stopped according to convergence checked on out-of-balance forces and/or displacements. If more detailed information are required (concerning for example the possibilities to solve thermo-mechanical-metallurgical problems), see Habraken *et al* [4].

The code being based on a Lagrangian approach, forging simulation could not be conducted to the end because of strong mesh distortions. Therefore, an automatic remeshing modulus has been developed.

The decision to remesh is based, either on a maximum relative number of over distorted elements detected by geometric criteria, or on error estimator based on Zienkiewicz proposed criteria. Then, a variable density mesh generator builds a new mesh according to the up-dated contour line and to local zones needing refinement or coarsening detected by the error analysis or geometric element criteria. Finally, a data transfer is performed between the old mesh and the new one. It is based on various interpolation schemes (Shepphard approach or old element search and interpolation). The practice has demonstrated that according to the type of simulations, different transfer methods induce a better rate of convergence at the simulation restart. Complete 2D thermo-mechanical simulations using up to 20 remeshing are now classically performed.

For deep drawing, 3D efficient solid elements either of sheet or brick type and their associate contact elements have been developed. For example, the solid mixed type element BLZ3D (8 nodes, 1 interpolation point) saves a lot of CPU time. Classically concerned with process where dynamic aspects can be neglected, the analyses use generally implicit static approaches, however explicit schemes have been introduced for deep drawing simulations taking advantage of classical tricks to decrease the number of time steps (artificial increase of punch velocity for instance). Numisheet benchmarks as well as local industrial comparisons give confidence in the approach. The above 3D element allows also 3D rolling simulation of quite complex shapes, (e.g. sheet piles) where 2D generalised state analysis cannot produced exact shape, or complex forging processes (e.g. the round-square dynamic forging of aeronautic rods).

It is to be noted that, in the field of steel design, this software

has been used for the modelling of beam-to-column connections in various contexts: see Bursi *and al* [5, 6].

## 3.2 The solid element

Several types of finite elements are available. In a classical axisymetrical problem, two displacement type parabolic 2D elements can be used, the PLXLS and the CPL2D. They can be described by 3, 4, 6 or 8 nodes and integrated by 1, 3, 4, 7 or 9 integration points. Global axes are chosen as well as Cauchy stress and strains. The axismetrical axis is the Y-axis.

The mesh is realised from the border to the centre of the solid. The mesh-maker creates a data file with the nodes and the elements of each part of the system. The degrees of freedom (DOF) and the material laws are still to be described at this step. The completion of the data file is manually done with the previous information but also with the remeshing information like the allowed number of distorted elements (see before). Then the completed data file is run in order to create the working files that allow stopping the calculation at any time and beginning again with another parameters.

## 3.3 The contact element

This is one main feature of the simulation for the studied problem. A complete description of the used element can be found in Habraken *et al* [7]. This special interface element is based on a penalty approach and derived from the virtual work principle. Kinetically compatible with the associated solid element, this element is defined by an isoparametrical approach and its numerical integration is carried out by Gaussian points. For some special choice of reduced integration scheme, this element is equivalent with a mixed one, based on a multi-field variational principle, see Cescotto *and all* [8]. The originality of the present approach lies in the fact that the contact conditions (Signorini's condition and Coulomb friction law) are expressed at some integration points, not at the nodal points.

The development of contact between deformable solids introduces a coupling between the degrees of freedom (DOF) of each body. A simple way to treat this kind of problem is to consider that at a given time t, the geometry of solid A is "frozen" and the contact elements belonging the solid B "see" the boundary of solid A as a rigid foundation. Reciprocally, at the same time t, the contact elements belonging to solid A are also calculated as if the geometry of solid B was "frozen". Hence, the contact forces computed by the contact elements of each solid depend only on the DOF of this solid. Consequently, the iteration matrix associated with a contact element does not establish any coupling between DOF of the solids. This approach will be termed as the "uncoupled approach". On the contrary, if the contact forces are computed exactly, they depend on the DOF of both solids and the corresponding iteration matrix establishes a full coupling between the DOF belonging to the boundary of both solids. This approach will be termed as the "coupled approach", according to studied contact both coupled and uncoupled cases which is applied on the swaging process simulation.

The contact law is related to elastoplastic formalism with an elastic field (sticking contact) bounded by a yield surface expressed by the dry Coulomb friction formula. The chosen friction coefficient was deduced from ring test experiments and simulations as explained in further section. So, the friction is computed with a penalized method, the contact modelled with specific elements [7]. ("u°" is the derived function for the time).

The contact is installed between a rigid solid called foundation and a deformable one. When the both are deformable, the formulation is quite the same. Then, the rate of stresses, $\underline{\sigma}^\circ$: $\{p^\circ; \tau_S^\circ; \tau_T^\circ\}$, is associated to the contact stresses, written as a vector of force divided by surface unit $\underline{\sigma}$: $\{p; \tau_S; \tau_T\}$. The rate of relative displacements of the borders is defined as well, $\underline{\varepsilon}^\circ$: $\{\varepsilon_R^\circ; \varepsilon_S^\circ; \varepsilon_T^\circ\}$. Notice that the p and $\tau$ components are respectively normal and tangent to the deformable solid surface. They are oriented with the orthogonal triedre {R, S, T}, defined at each integration point. The penalty relation between the both rates is given by:

$$\underline{\sigma}^\circ = \underline{C}\,\underline{\varepsilon}^\circ \qquad (1)$$

where $\underline{C}$ is a symetrical diagonal matrix in a stick contact case or a non-symetrical matrix in a sliding contact case. The computation of the friction law, based on the Coulomb law, is realised as a elastoplastic one is, that is as an irreversible phenomena. Then, the graph of the different domains marked by the sliding function, $f = (\tau_S^2 + \tau_T^2)^{0.5} - \phi.p$ where $\phi$ is the friction factor, is given Figure 3.

In metal plasticity (standard or associated plasticity), the normality law is used to express the plastic strain rate:

$$\underline{\dot{\varepsilon}}_p = \dot{\lambda}\left(\frac{\partial f}{\partial \underline{\sigma}}\right) \qquad (2)$$

where $\lambda^\circ$ is the plastic factor. But, this law cannot be kept because no strain is associated to the contact pressure.

That's why, a non-associate plasticity law is employed as the flooding law. The function f is replaced by another function:

$$g = \sqrt{\tau_S^2 + \tau_T^2}\,. \qquad (3)$$

Then, the hardening factor $\mu$ can be evaluated with the equations:

$$f^\circ = 0 \qquad (4.1)$$

$$\lambda^\circ = \mu.\frac{\partial f}{\partial \sigma_i}.\sigma_i^\circ \qquad (4.2)$$

The penalty relation can be written as:

$$\sigma_i^\circ = C_{ij}^e.\varepsilon_j^\circ - \lambda^\circ.C_{ij}^e.\frac{\partial g}{\partial \sigma_i} \qquad (5)$$

where $C_{ij}^e$ is the diagonal matrix of penalty coefficients.

The finite elements for the contact are 1st or 2nd order isoparametric. All the parameters (geometry, stresses, local axes) are determined at their gaussian nodes. These elements are respectively linear or surface if the simulation is 2D or 3D. For each integration point of the solid surface, the contact is to be found. This determination is based on the existence of a penetration between the foundation and the solid but also on the sign of the scalar factor of the contact point normals (Figure 3).

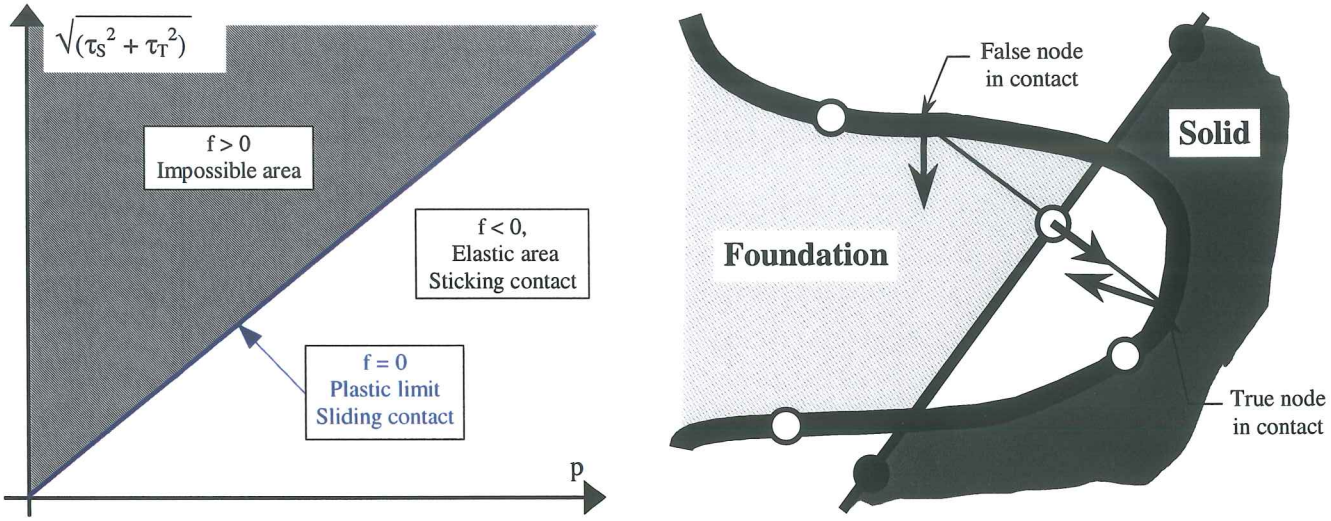


Figure 3: Contact domains and determination method of the nodes in contact

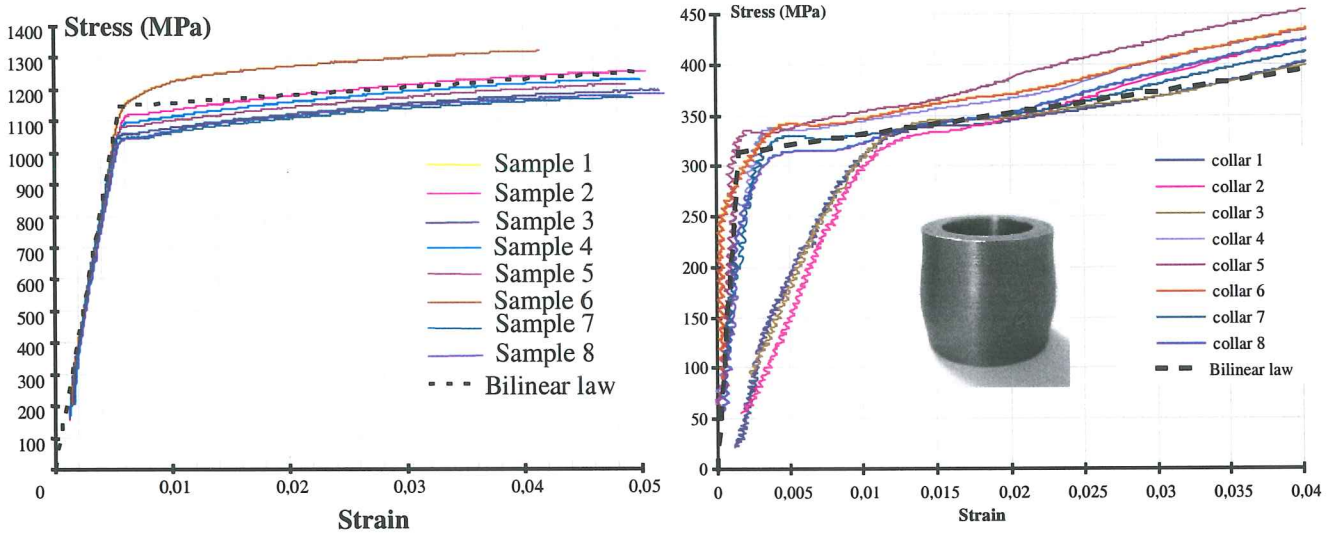


Figure 4: Strain-stress curves of the pin and strain-stress curves of the collar

The finite elements for the contact are 1st or 2nd order isoparametric. All the parameters (geometry, stresses, local axes) are determined at their Gaussian nodes. These elements are respectively linear or surface if the simulation is 2D or 3D. For each integration point of the solid surface, the contact is to be found. This determination is based on the existence of a penetration between the foundation and the solid but also on the sign of the scalar factor of the contact point normals (Figure 3).

## 3.4 Mechanical characteristics of swaged bolts

During the installation, permanent deformations are observed in the collar. They are due to the laminating of the anvil. Several mechanical phenomena can be remarked: the elastoplastic behaviour of constitutive steels, the friction contact between the anvil and the collar, the damaging of the breaking groove and the chock which results of the break of this groove.

**Mechanical characteristics of the pin.** The dimensions of the pin are sufficient to allow standard tension samples to be extracted. Some tests have been performed by Czarnomska *et al* [1], some others have been obtained more recently [9]. They can be represented by a bilinear law. Their mechanical characteristics are given in table 1 (Figure 4).

**Mechanical characteristics of the collar.** Because of the small sizes of the collars, it is much more difficult to obtain classical tension samples .So it was decided to carry out compressive tests from cylindrical samples easily extracted. This testing series presents two aspects. The first one is the crushing test of the cylindrical sample measuring the displacement of the moving table. Then, the second aspect is a test (white test) without a sample in order to measure the flexibility of the testing machine. The values of displacement of both tests are subtracted for the same value of crushing effort. The results (Figure 4) are the nearest of classical steel values from the whole tests.

**Mechanical characteristics of the steel plates.** The steel plates are made from S235 steel grade. No strain hardening is taken into account.

| | Young's modulus | Yield stress | Strain hardening modulus |
|---|---|---|---|
| Pin | 210 200 MPa | 1 170 MPa | 2500 MPa |
| Collar | 204 200 MPa | 313 MPa | 2090 MPa |
| Plates | 210 000 MPa | 235 MPa | 0 MPa |

Table 1: Mechanical characteristics of each component

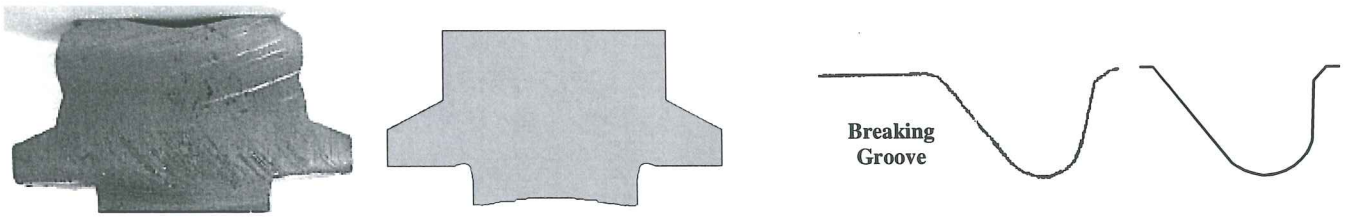


Figure 5: Real and modelled shapes of the pin-head and of the breaking groove

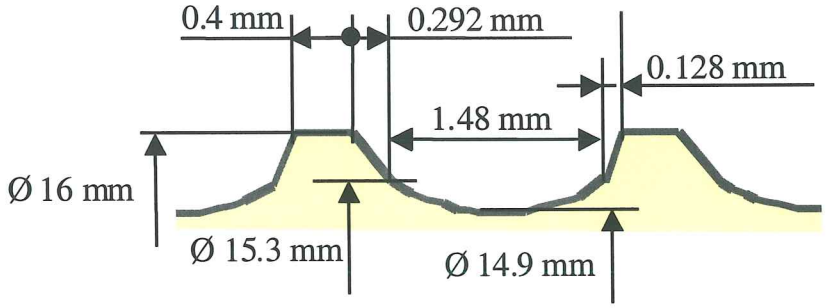


Figure 6: Thread dimensions

As poor knowledge on the constitutive material is available, it was chosen to do not use the damage law, which could have better modelled the pin rupture. A classical elastoplastic law of von Mises type with simple bilinear stress-strain curve was adopted. All the considered mechanical characteristics of the whole model are given in the table 1.

**Mechanical characteristics of the friction**. A good modelling of the installation must take into account the efforts transmitted by the friction between the anvil and the collar. To define the mechanical characteristics, a measure of the barrel deformation of the samples cut in collars is realised after the crushing tests. The covering on the sample support surfaces was kept to approach as close as possible the real conditions between the anvil and the collar. Then, to evaluate the mechanical characteristics resulting from this test, a numerical model of the sample has been computed. It is associated with different values of the friction coefficient $\phi$ existing between the sample and the testing machine supports but quite impossible to measure. Comparing the stress and the final shape, it is possible to qualify the best value for this coefficient. The 0.05 value has been chosen for the friction coefficient as well as a bilinear law. The 0.15 value has been chosen for the other contact of the model (plates/pin, plates/collar and pin/collar).

# 4 Modelling

## 4.1 Geometry of the bolt

The bolt shape leads to the chosen axisymetrical model. The hexagonal flange of the collar and the head of the pin are approximated to cylinders with the same normal sections (Figure 5). The profile of the head is kept but a same normal section cylinder replaces the hexagonal part. The equivalent diameter $\phi_{eq}$ is calculated with a formula where $\phi_{ins}$ is the diameter of the inscribed circle and $\phi_{cir}$, the drawn round circle diameter:

$$\phi_{eq} = \sqrt{\left(\frac{3\,\phi_{ins}\,\phi_{cir}}{\pi}\right)} \qquad (6)$$

The helical grooves of the pin are transformed into fluting but keeping the real non-symmetric profile. All the dimensions are chosen as close as possible from the theoretical or nominal manufacturer data and from data obtained by profile projections (Figure 6). The pintail keeps its real length, 54 mm. And, to respect the full mechanical behaviour during the installation, the breaking gorge is also represented as real as possible (Figure 5). The dimensions of its profile are obtained with profile projection.

The collar, as well as the pin, is more or less cylindrical. As modelled in the pin, the hexagonal flange is replaced by a equal normal section cylinder in order to keep the same contact area (Figure 7). The dimensions are also taken from profile projection measures.

## 4.2 Geometry of the plates

A lonely cylinder models the plates. The value of its external diameter is chosen big enough to allow the stresses to have a realistic diffusion. The manufacturer gives the value of the internal diameter.

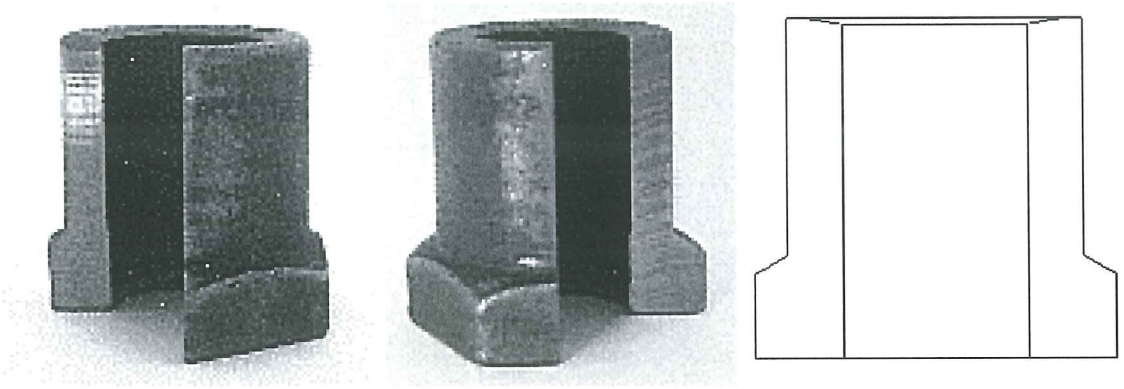

Figure 7: 16 mm diameter collar: real and modelled shapes

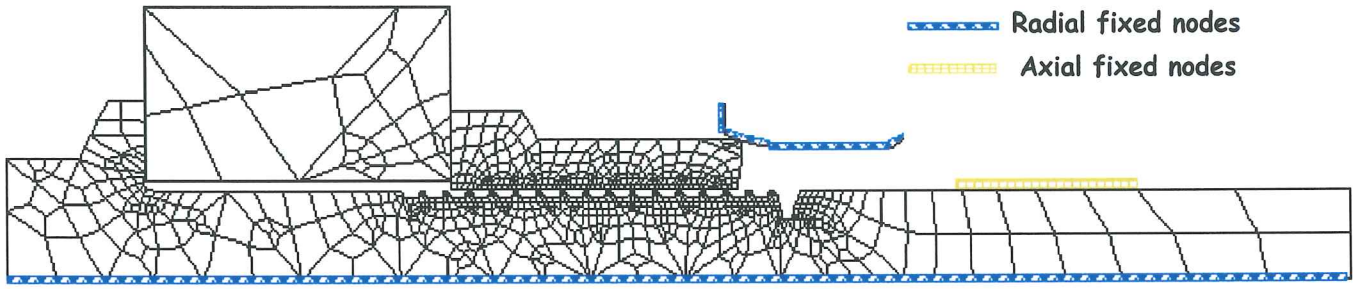


Figure 8: The final whole model

## 4.3 The whole geometry

«Lagamine» being developed for metal forming, it must be able to follow the different steps occurring during swaging. Nevertheless, because some mechanical characteristics of the bolts are not known with a sufficient precision, it is necessary to calibrate the model carefully. At first, it was thought that remeshing would be necessary but practice shows that this could be dropped.

Figure 8 shows the whole modelling including the pin, the collar, the steel plates (represented by one piece of steel) and the tool.

## 4.4 Strategy of computation

In order to calibrate the parameters governing the mechanical behaviour of the installation process, it was necessary to define some reference steps. Because it is not possible, at this time, to measure the forces developed by the hydraulic tool during the installation, the first reference step is chosen to be the displacement of the anvil by the body of the installation tool. During the installation tests, a transducer fixed on the body of the hydraulic tool (Figure 8) measured the displacement of the anvil (graph on Figure 8). Point A marks the creation of the first thread in the collar. The swaging process ends at point B, point C represents the stop of the anvil. The break of the pintail occurs at point D and the coming back of the tool begins at point E.

Then, the loading follows the evolution of the forces applied to the body of the installation tool. This strategy is chosen to be as close as possible to the real installation process. The hydraulic power unit imposing the pressure on the piston, it creates the force on the anvil. The calculation is carried out into two steps. The first one is the swaging of the collar onto the pin (Figure 8, between A and B), the second one is the disengagement of the tool from the collar (Figure 8, after E).

The loading is assumed by the controlled displacement of the anvil. This choice, chosen in order to favour the computation convergence, does not represent the reality of the installation. Indeed, in the hydraulic tool, the pressure is imposed, which is closer of force leading. But, this leading control causes convergence problems. So, the whole presented results come from computations with displacement leading.

## 4.5 Representation of the contacts

Concerning the contacts, different ways were tested. The conclusion of these tests is that the best modelling method, if not the possible one, is the coupled approach without privilege, mainly because the stiffness of each solid are very close (except the anvil).

## 4.6 Computations

The computations were made in two series. The first one was done to check the validity of the software choice. The second one was a large study of parameter influences. The calculations were done with Digital workstations and VMS operating system. During the time of the study, the computers improve from an *ALPHA 4000* workstation to an *ALPHA 350-600* workstation. The calculations CPU-times decreased from almost five days to less than 24 hours.

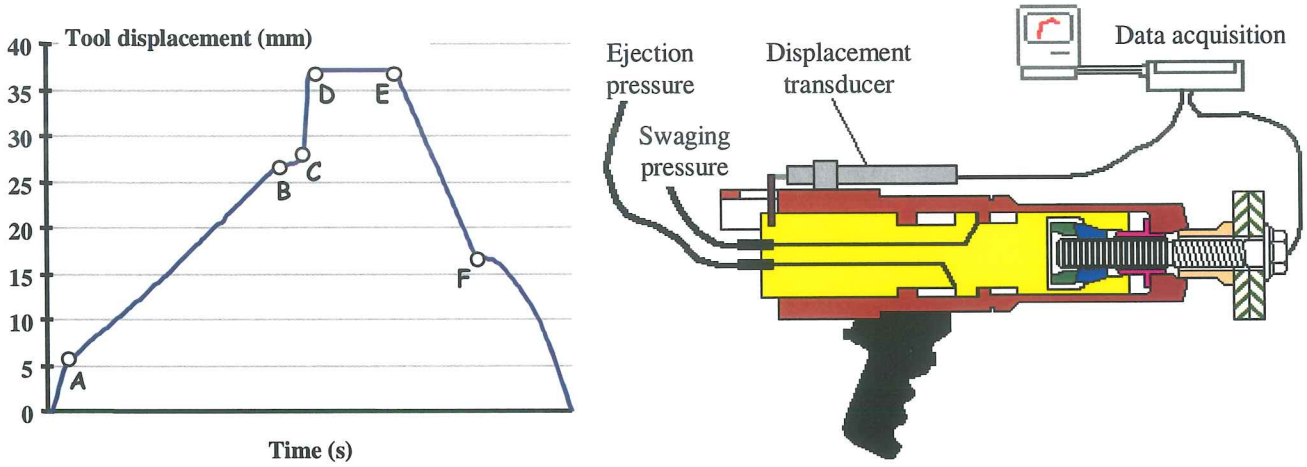


Figure 9: Measured displacement of the hydraulic tool and experimental equipment for the installation test

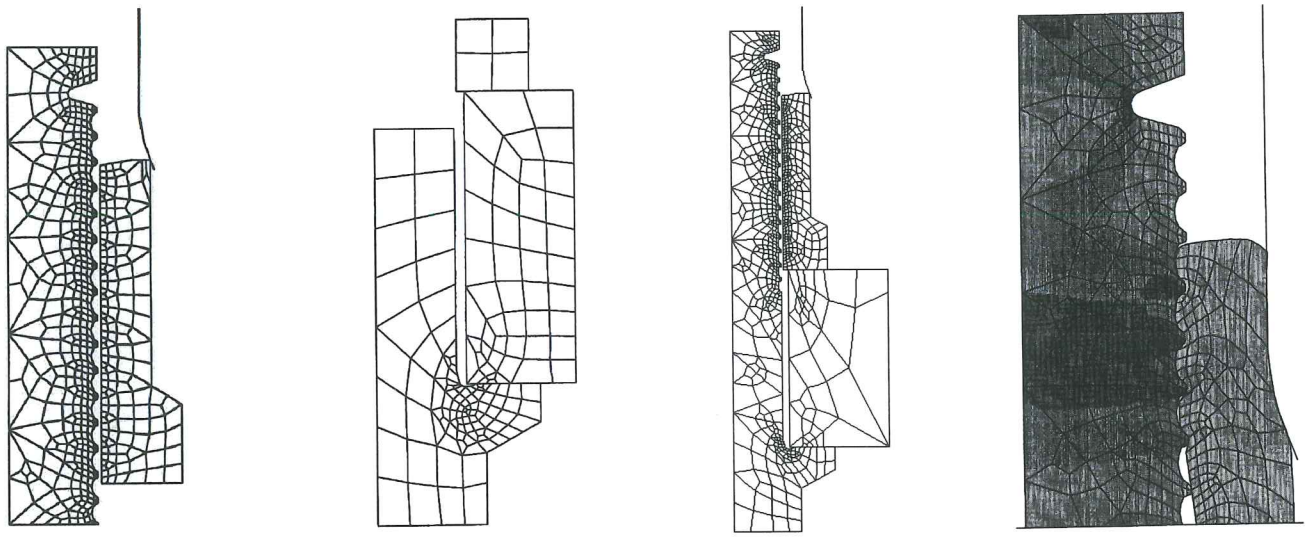

Upside model | Downside model | First whole model | First computation results

Figure 10: First tests of computation meshes

During the second period of calculations and to allow modifying the numerical conditions of the computation, the whole-modelled swaging process is divided in three steps. Indeed, the starting up of the calculation reveals to be critical, due to necessary initial penetration to install between the anvil and the collar. The pre-existing effort generates a numerical bound due to the contact strategy. Lowering the non-equilibrated forces attenuates this effect but slows the computation. Then, in the following, this effect is reduced. The choice of the loading step is automatically adapted within the performance of the convergence. Only the minor value and the major value of this step are determined at the beginning. In order not to fill up hard disk drives, results were kept for only few anvil displacement values.

# 5 Results

## 5.1 First computations

During the first period of calculations, the model has been tested separating it into two parts, the upside part with the collar and the downside part with the head pin and the plates (Figure 10).

The both computations were led to check that the contact stack would not be too unstable and lead to divergence. The results showed that each part could be calculated during the swaging process but also during the anvil withdraw.

The deformations of the meshes are quite the same as the real bolt. The penetration allowed between the meshes is reduced for the last period because it is far too much in this case.

The influence of the pintail size appears to be so big that it was decided to keep the real length and the real shape in the final period. Indeed, the stresses flow is better respected with a long pintail and with fixed nodes further placed on the pintail.

## 5.2 Swaged geometry of the final model

Comparisons are made on the collar geometry. The shape of the collar mesh at the end of the numerical installation is compared with the shapes of a real swaged collar cut in the middle (Figure 11).

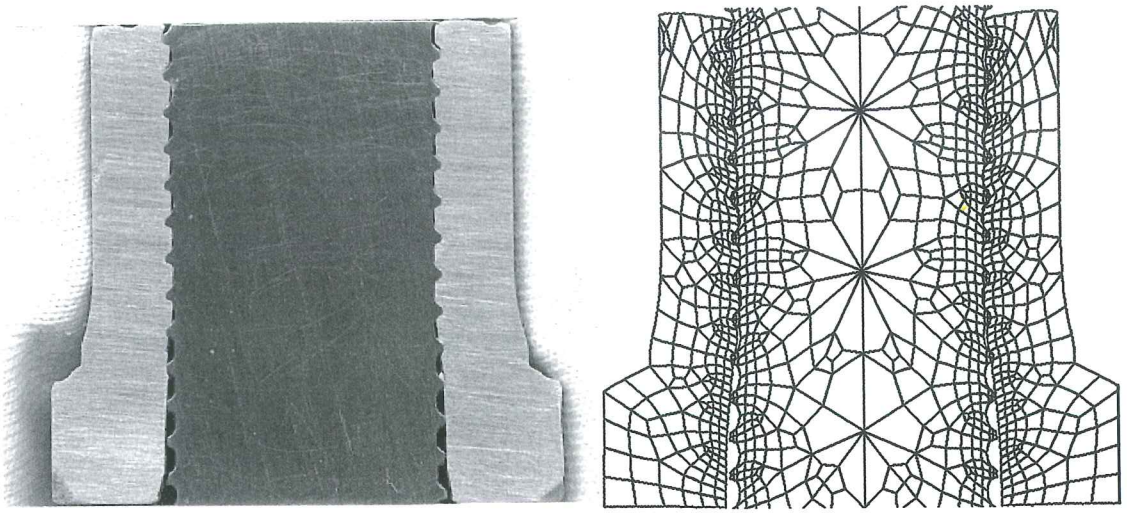

Figure 11: Cut sample of swaged bolt and mesh at the end of the numerical installation

| Data type | Swaged diameter at the collar top (mm) | Swaged length (mm) |
|---|---|---|
| Test average | 23.97 ($\sigma$ = 0.012) | 19,9 ($\sigma$ = 0.23) |
| Modelling results | 23.98 | 20.35 |
| Control data | 24.1 maxi | 17.7 mini |

Table 2: Geometrical dimensions taken on the swaged collar

The mesh matches very well with the filling up of the real pin threads. Indeed, the threads at the top of the collar present gasp with the pin, because of the hold of the anvil on the flange of the collar at the end of the swaging process. The threads in the middle are better shaped and filled in. The threads at the bottom of the collar are nearly absent. In fact, the threads begin at the top of the collar flange.

The compared dimensions are the ones that have to be controlled. But, there is no break of the pintail. So, it is difficult to measure the length of the pin that is out of the collar, after the installation.

The comparison takes place on the external diameter of the collar after the installation and on the swaged length of the collar. The diameter values of the modelled swaged collar vary from 23.98 mm at the top, to 24.14 mm at the bottom. The experimental values can only be measured at the top because of the accessibility of the calliper rule. The swaged length is measured with a ruler and according to the manufacturer method. All the experimental values match with the control values and verify quite well the numerical modelling values (Table 2).

## 5.3 Efforts during the installation

**Preload effort.** Installation tests have been used to compare the numerical results to the real behaviour. They consist in measuring the preload in the pin as well as the displacement of the anvil during the installation. The preload is red with an axial gauge placed in the shank zone of the pin (Missoum [2]). This gauge is calibrated to answer directly in kN. A displacement transducer (Figure 9) measures the displacement on the hydraulic tool. So, it is possible to obtain a preload-displacement curve (Figure 9).

These data are used in the computation. The tension in the pin is deduced from the stress value obtained in the finite element corresponding to the gauge location. The displacement is chosen to be equal to the tool displacement. So, another preload-displacement curve can be obtained. If the computation were governed by force, the displacement would be taken from the one of the installation tool. This strategy is not presented in this paper.

Even if the curves keep the same global shapes, some differences appear about the final preload. The loss of preload observed on the numerical curves can be explained by the strategy of computation. Imposing the displacement allows the material to flow; that creates a decreasing of forces. The differences of loading levels at each step of the installation are due to the variations of the mechanical characteristics and of the dimensions of the tool. Notably, the level of preload at the end of the loading is mainly sensible to the value of the strain hardening modulus of the pin. Regarding the preload at the end of the tool ejection, it appears to be lower than the real value. The dimensions, but also the shape, of the tool are very relevant to this preload.

According to these numerical results and experimental results, a comparison of the tensile efforts in the pin is led for each key-step of the installation. (Table 3). The only anvil removal phase is not mentioned because it corresponds to a variation of the tensile effort. The comparison of these different values shows that the dimension order between the experimental data and the numerical data is kept.

**Internal efforts of contact during the installation.** To verify the equilibrium of each modelled connection solid, the contact efforts between the solids are calculated and represented (Figure 12). The contact effort between the collar and the plates is not drawn because it is equal to the contact effort between the pin and the plates.

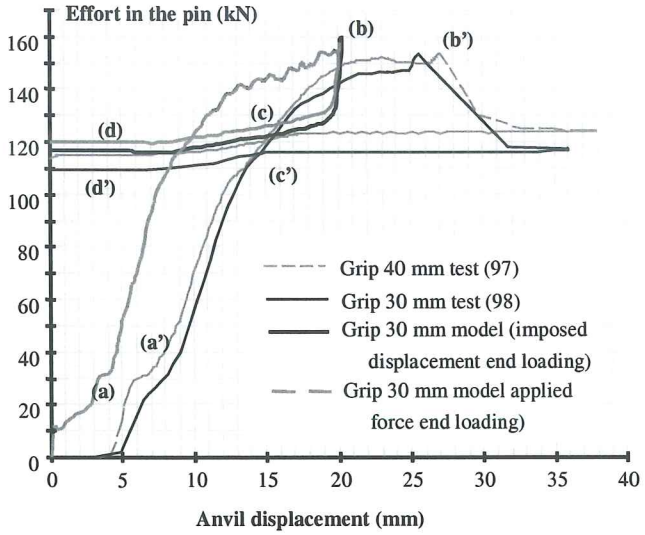


Numerical and experimental preload-displacement curves

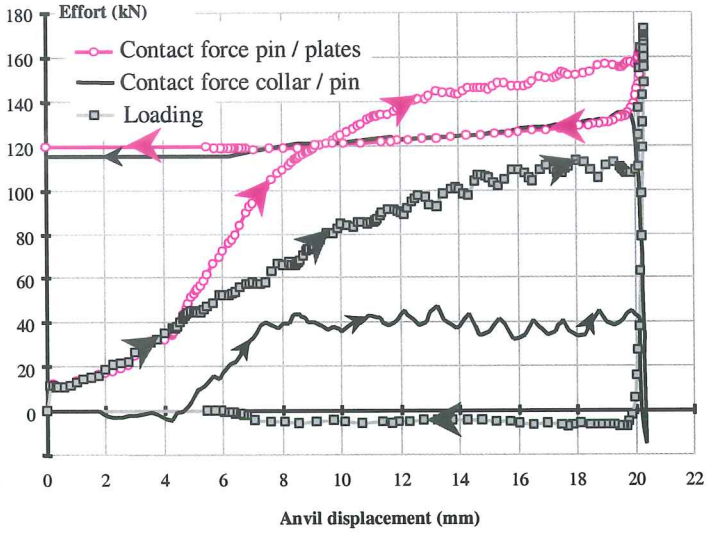


Computed forces between the different components of the bolt

Figure 12: Compared results and analysis curves during the installation of a swaged bolt

| Source | Major effort in the pin **(b)** (kN) | Final preload **(d)** (kN) | Effort loose at the pintail "break" (kN) |
|---|---|---|---|
| 40 mm grip test | 154.6 | 114.8 | 39.8 |
| 30 mm grip test | 148.9 | 105.6 | 43.3 |
| 30 mm grip model (displacement stop) | 159.6 | 117 | 42.6 |
| 30 mm grip model (force stop) | 157.8 | 120.25 | 37.55 |
| Manufacturer documents | - | > 113.4 | - |

Table 3: Efforts in the pin at the key moments of the installation

During the swaging process, the axial contact effort between the plates and the pin is the addition of the contact effort between the pin and the collar and the loading effort. Three forces apply on the pin, which is mechanically equilibrated during the swaging process. Also, the effort in the pin is bigger than the loading effort. The difference is due to the collar expansion, which generates a part of the preload. The other part is generated by the hold of the loading effort.

Then, during the anvil removal, the loading effort applied by the anvil becomes negligible. So, the contact effort between the collar and the pin has the same values as the contact effort between the other solids has (plates/collar and plates/pin). Two efforts equilibrate each solid, which are equal. That statement confirms the good mechanical equilibrium of the model.

Figure 13 presents the ways taken by the efforts between the solids during the installation of a swaged bolt. Before the creation of the first thread in the collar and so, before the creation of the contact effort between the collar and the pin, all the solids are mechanically equilibrated by two forces. That is why, the axial projections of these efforts are all equal, notably the loading effort and the effort in the pin. During the swaging process, a new force appears between the pin and the collar. At the beginning of this process, this force reacts against the loading effort. But, when the threads in the collar are stronger enough, the contact force between the collar and the pin changes and adds to the loading effort. This change of sign is due to the axial expansion of the collar limited by the plates and the threads.

At the pintail break, the loading effort moves to the contact between the collar and the pin. And also, two forces mechanically equilibrate the solids.

The anvil removal shows a little effort due to the friction between the anvil and the collar. The last equilibrium is not modified by this effort because it is too small. The loose of force in the pin comes from the released circular stress.

## 5.4 Stresses in the bolt during the installation

A strong stressed area can be remarked, following the displacement of the anvil during the swaging process (Figure 14).

At the beginning of the anvil removal, the stress in that area reaches a value nearly equal to the stress in the breaking groove. Then, the strong stressed area stays at the same place but the value of axial stress has decreased. That position in the pin is quite the same of the position of fatigue fracture appeared in fatigue tests on that bolts, Missoum [2].

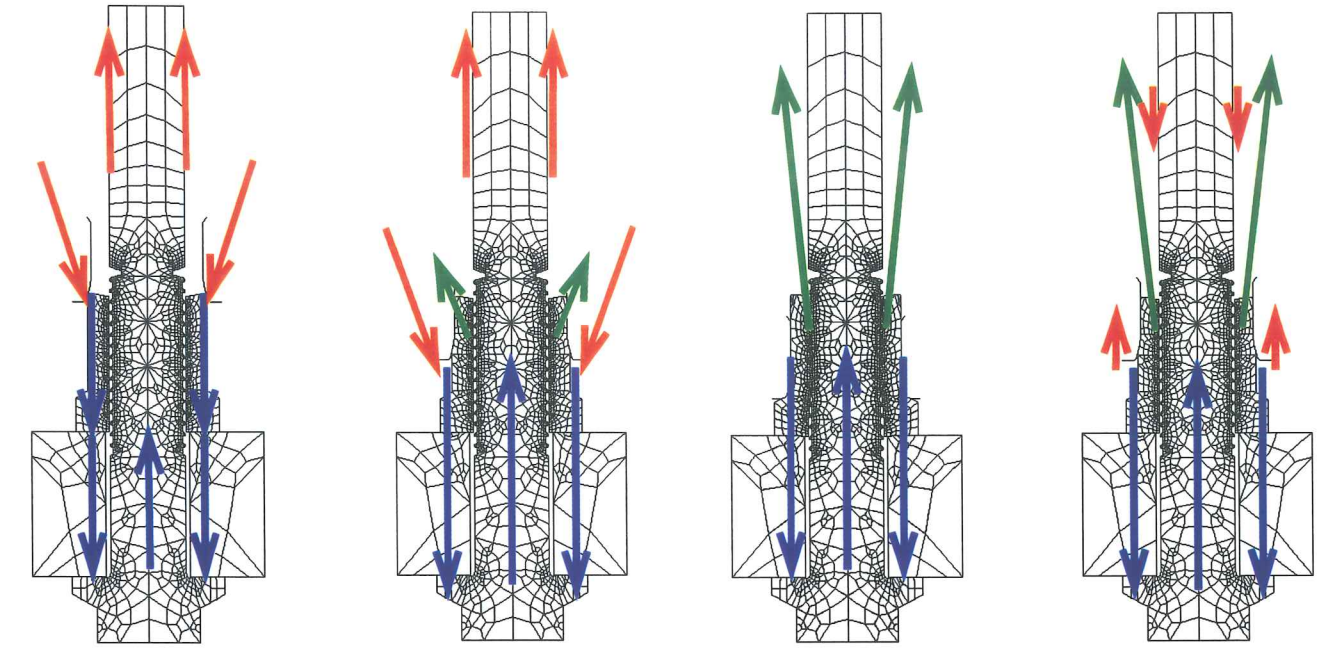

Before the first thread creation | During the swaging process | Just after the pintail break | During the anvil withdraw

Figure 13: Effort paths between the solids in the swaged bolt

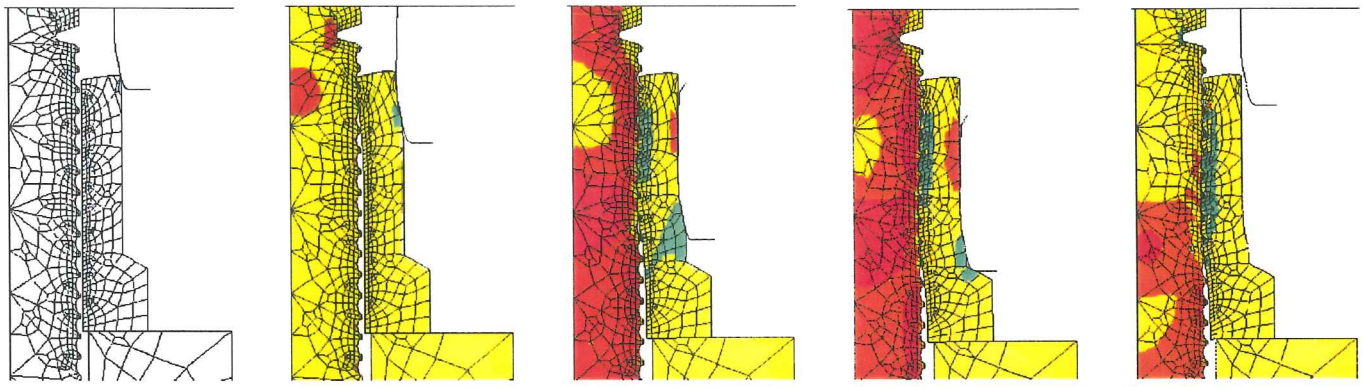

Single mesh | During the swaging process | At the beginning of the anvil withdraw | At the end of the anvil withdraw

Figure 14: Axial stresses in the model

## 6 Conclusions

Modelling of the installation process of swaged bolts represents several mechanical steps, steps that cannot be approach by tests. This is due to the facts that the size of the collar does not allow a fine instrumentation to be installed and that the constitutive steel characteristics are strongly modified during the installation. So, a numerical model is required which needs to involve a simulation technique able to represent the large strains associated with the collar forming process on the tail.

In a first phase, a detailed modelling of a swaged bolt has been defined; it considers both the pin and the collar. Then, the software «Lagamine», based on the FEM and especially written for large distortions and large displacements, has been chosen to compute all the mechanisms involved during the different swaging steps.

The pin, the collar and the steel plates are modelled as close as possible to their actual shape and to their accurate mechanical characteristics, these last being deduced from several tension or crushing tests refined with a numerical analysis.

To represent the real shape of the anvil, the modelling of the tool is carried out using rigid lines. Its displacements govern the computation. The Coulomb friction law is used to model the contact between the different meshes. The numerical results are compared to the experimental ones, which are carried out by measuring the force with a strain gauge located in the shank zone of the pin. The differences, which appear in the general behaviour, are due to the difference between the mechanical characteristics taken for the computation and the actual ones. This allows the sensibility of some parameters to be evaluated (the strain hardening of the pin or the tool shape for instance).

This numerical approach gives a very efficient information about the behaviour of the bolt at each step of the installation process. It allows the detailed stress distribution to be established with a reasonable accuracy. That leads to a better

understanding of the parameters acting a role in the mechanical behaviour of this new fastener, and clarifies the sensibility of the collar swaging process.

This study shows that the characteristics of each component (pin or collar) have a strong influence on the mechanical behaviour during the installation, but also that the diameter, and more surprisingly the shape of the tool, is also very influential on the history of the preload value.

## References


[1] Czarnomska M., Muzeau J.P. and Racher P., Étude expérimentale comparative du comportement d'assemblages par boulons sertis Huck-Fit ou par boulons hr 10.9. *Construction Métallique*, 1993, **2**, 9-29.

[2] Missoum A., Étude expérimentale de boulons sertis précontraints utilisés en Construction Métallique, *PhD Thesis, Blaise Pascal University*, Clermont-Ferrand, France, July 1997.

[3] Baptista A.M., Missoum A., Muzeau J.P. and Ryan I., Testing of swaged bolts for steel connections. *International Conference "New Technologies in Structural Engineering", NEW TECH'97*, Lisbon, Portugal, 1997, 589-594.

[4] Habraken A.M., Bourdouxhe M., Coupled thermo-mechanical-metallurgical analysis during the cooling of steel pieces. *European Journal of Mechanics, a: Solids*, 1992, **11**(3), 381-402.

[5] Bursi O.S., Jaspart J.P., Basic Issues in the Finite Element Simulation of Extended End Plate Connection, accepted in *Journal of Structural Engineering*.

[6] Bursi O.S., Jaspart J.P., Finite element-based models for the analysis of bolted beam-to-column steel connections. *Colloquium Istanbul 96 "Semi-rigid Structural Connections" published by IABSE-AIPC-IVBH ETH-Hönggerberg Zürich*

[7] Habraken A.M., Cescotto S., Contact between deformables solids, the fully coupled approach. *to appear in a special issue of Mathematical and Computer Modelling, 1998.*

[8] Cescotto S., Charlier R., Frictional Contact Finite Element Based on Mixed Variational Principles. *Int Journal of Numerical Methods in Engineering*, 1993, **36**, 1681-1701

[9] Dréan M., Modèle numérique du sertissage de boulons sertis utilisés dans des assemblages de constructions métalliques, *PhD Thesis, Blaise Pascal University*, Clermont-Ferrand, France, January 1999.